# pH and anion effects on Cu-phosphate interfaces for CO electroreduction

*Paula Sebastián-Pascual, Amanda S. Petersen, Alexander Bagger*, Jan Rossmeisl, and María Escudero-Escribano**

Department of Chemistry, University of Copenhagen, Universitetsparken 5, 2100 Copenhagen, Denmark

*Corresponding author:

E-mail: maria.escudero@chem.ku.dk

E-mail: alexander@chem.ku.dk

## ABSTRACT

Cu electrodes are promising materials to catalyze the conversion of $CO_2$ and CO into renewable fuels and valuable chemicals. However, detailed description of the properties of the Cu-electrolyte interface is still crucial to reach a complete understanding of the CO reduction mechanism. Herein, we have investigated the interfacial properties of Cu(111) and Cu(100) in phosphate buffer solutions at different pH conditions and in presence of CO. Ab initio molecular simulations of the Cu-electrolyte interface were combined with voltammetric experiments carried out on Cu(100) and Cu(111) single-crystalline electrodes. Combining multiple cyclic voltammograms on Cu single crystals across the whole pH scale with simulations allows for an in-depth insight into the stability of specifically adsorbed protonated ($H_2PO_4$* or $HPO_4$*) or non-protonated ($PO_4$*) phosphate species from the electrolyte. We show that the adsorption strength of phosphate species on the different Cu facets affects the potential range at which CO poisons the surface, thus evidencing that the properties of the Cu-electrolyte interface control the potential range for CO reduction on Cu. This combination of systematic experimental and theoretical analysis across the pH scale is a robust method to gain fundamental structural insight of electrochemical interfaces.


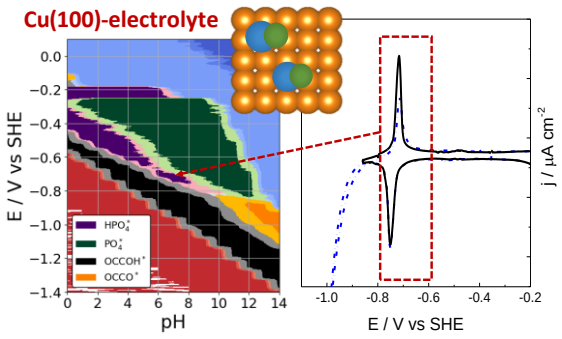


**Table of contents graphic**

## Keywords

Electrocatalysis, electrochemical interface, CO reduction, pH effects, electrolyte effects, cyclic voltammetry, ab initio molecular dynamics simulations

## Introduction

Selective and efficient conversion of greenhouse gases such as carbon dioxide ($CO_2$) into green fuels and chemicals is one of the most important technological and environmental challenges that the society is currently facing.[1–3] Electrocatalytic $CO_2$ reduction ($CO_2RR$) is a sustainable alternative to convert $CO_2$ into renewable fuels and valuable chemicals, allowing for the transition to a decarbonized scheme of energy.[4–6] Up to date, copper is the only pure metal catalyst that can reduce $CO_2$ beyond carbon monoxide (CO), producing a wide range of fuel alcohols and hidrocarbons.[7–9] In parallel, studies dedicated to investigate the CO reduction reaction on Cu have provided indirect insights for deeper understanding of the $CO_2RR$.[10–16] The pioneering work by Hori and co-workers on electrocatalytic CO reduction on Cu in the 80s[10,16] have inspired our community for the search of a rational explanation of the reaction mechanism, that continuous to be a focus of debate. In particular, the use of model Cu surfaces such as single-crystalline electrodes, has represented a progress in the understanding of both the $CO_2RR$ and the CORR, allowing to find the relations between electrocatalytic performance, surface structure and electrolyte effects.[12,13,17–24]

There is a large number of reports that have analyzed electrolyte effects on the CO reduction,[6,14,23,25,26] as well as the effect of the local pH change on the catalytic performance of Cu catalysts. The latest is particularly relevant as the interfacial pH affects the product distribution on the CO reduction.[25,27–29] Thus, assessing the effect of both the solution pH and specific anion

adsorption on the minimum required potential for the CO or its intermediates to remain stable on Cu single crystalline electrodes is essential for detailed description of the CORR.[12,22,30,31] Noteworthy, both pH and electrolyte effects have been widely investigated in other electrocatalytic reactions of interest, such as the oxygen reduction reaction on Pt,[32–35] evidencing the key role of the pH and selected electrolyte while assessing the performance of an electrocatalytic reaction.

Hori and co-workers investigated the effect of the pH on the adsorption of CO on different Cu single-crystalline surfaces at low temperature and in phosphate buffer solutions.[30,36,37] They observed that CO weakly adsorbs on Cu, inducing the appearance of a quasi-reversible pair of voltammetric peaks, which corresponded to the competing desorption/adsorption reaction between either the protonated or non-protonated electrolyte anion, and the CO molecules.[30] In CO-saturated phosphate buffer solutions, assuming a reduction reaction, the elementary displacement reaction occurring is:

$$H_mPO_4^* + CO \ + |n-m|H^+ + |3-m|e^- \rightleftharpoons H_nPO_4^{-3+n}(aq) + CO^* \qquad (1)$$

where $CO^*$ and $H_mPO_4^*$ are the stable CO and phosphate adsorbates, and $H_nPO_4^{-3+n}$ corresponds to the dominant phosphate specie in solution. The parameters *m* and *n* are chosen according to the protonation of the phosphate anion adsorbed and in solution, respectively. The charge of the adsorbate is assumed neutral.

Assuming that, in the previous proton-coupled electron transfer reaction (1), the electrochemical equilibrium is achieved, the CO-peak potential value would approach linearly to the pH, according to the Nernst equation in the 10-log form, as follows:[38]

$$E_{CO-peak} \approx 59.2\ mV \cdot \frac{|3-m|}{|n-m|} \approx 59.2\ mV \cdot \frac{y}{x} \qquad (2)$$

with $x$ being the number of transferred protons, and $y$ the number of transferred electrons in the reaction.

The experimentally obtained slope ($59.2\ mV \cdot y/x$) is an indicative parameter to shed light on the chemical nature of both adsorbed species and species in solution in the CO-saturated electrified interface. Hori and coworkers observed that the voltammetric CO-peak on Cu(100) linearly shifted approximately 30 mV per pH unity,[30,36] from which they concluded that $HPO_4^*$ and $PO_4^*$ were the main adsorbed species on the surface competing with the CO. The potential value of the voltammetric CO-displacement peak depends not only on the employed electrolyte and solution pH, but also on the surface orientation. Recently, we analyzed the voltammetric features of Cu(111) in different electrolytes and under the presence of CO.[23] Our work showed that the main singular voltammetric features, obtained in presence of CO, were highly affected by both the selected electrolyte and the surface structure.

Herein, we combine ab initio molecular dynamics (AIMD) simulations with cyclic voltammetry carried out on Cu(100) and Cu(111) single-crystalline electrodes, to shed lights into the Cu | electrolyte interface properties, and their effect on the onset potential of the CORR. Both simulations and voltammetric experiments were conducted on Cu(111) and Cu(100) in contact with phosphate buffer electrolytes, covering the whole pH scale. This study provides rational description of the Cu-electrolyte interfacial properties, and show that both pH and electrolyte anions play a key role in controlling the potential windows for electrocatalytic CO reduction.

## Results

Cyclic voltammograms (CVs) of both Cu(100) and Cu(111) | 0.1M phosphate solution interface in presence of CO were assessed. Figure 1A shows the voltammogram windows of Cu(100) in contact with CO-saturated phosphate solutions. The recorded CVs across the whole pH range display a quasi-reversible pair of peaks located in the low potential window, *i.e*. close to the solvent and CO co-reduction potential limit (Fig. 1A, potential range between -0.65 V and -0.9 V vs SHE). These voltammetric features correspond to weakly adsorbed CO that replaces the phosphate anions adsorbed on the surface by means of the CO-displacement technique. These results are in agreement with earlier work by Hori and co-workers.[30,36] Notably, these peaks shift to more negative potential values by increasing the pH of the solution in the standard hydrogen electrode (SHE) scale, showing the pH influence on the voltammetric curves. On the other hand, the hydrogen evolution reaction (HER) on the surface slightly reduces the reversibility of the CO-anodic peak (see blue line, Fig. 1A), which shifts to more positive potential values. This is likely due to surface restructuration or reconstruction induced by the HER, which affects the voltammetric profile.[39–41] The irreversibility on the peaks is reduced by shortening the potential window (black lines, Fig. 1A). In contrast to CVs recorded in presence of CO, blank CVs of Cu(100) do not display any feature in the pseudocapacitive region in acidic and neutral pH (see Fig. S1A from the supporting information (S.I.) material, potential range between -0.2 V to -1.0 V vs SHE, pH<8). The absence of voltammetric features is due to the fact that phosphate adsorption in the blank CV of Cu(100) overlaps with the HER currents.[30] Under the presence of CO, the characteristic CO-displacement peak appears because the CO poisons the surface, broadening the potential window. In contrast, at alkaline enough pH, the Cu(100) blank CV shows a quasi-reversible peak which is related to the phosphate adsorption on the surface (Fig. S1A, potential

range between -0.94 V to -1.00 V vs SHE, pH > 8). The presence of CO in solution slightly shifts the phosphate peak to higher potentials, indicating that CO adsorbs on the surface at potentials close to the phosphate desorption potential region.

Figure 1B shows the potential windows of the Cu(111) | 0.1M phosphate at different pH and under the presence of CO. The short potential windows (black line, Fig. 1B) display the quasi-reversible pair of peaks on this crystallographic orientation, and related with the CO adsorption on Cu(111) (peaks are located in the potential region between -0.53 V and -0.70 V vs SHE). [23] Unlike Cu(100), the blank CVs recorded on Cu(111) display the pair of peaks, addressed to adsorbed phosphate, at low pH up to 4 (Fig. S1B, potential region between -0.55 V to -0.72 V vs SHE ). This is because, on Cu(111), phosphate desorption occurs at considerable higher potentials well separated from the HER potential limit. As evidenced in Figure 1B, the presence of CO in solution modifies the main voltammetric features of the blank CVs,[23] and slightly shift the phosphate peak towards more positive potential values due to the weak CO adsorption on Cu(111). Importantly, broad potential windows (Fig. 1B blue lines), *i.e.*, scanning to more negative potential that the onset of the HER, highly affect the voltammetric profiles in the anodic scan (potential limits ranging between -0.85 V to -1.4 V vs SHE by increasing the pH from 4 to 12). In particular, both the anodic CO and phosphate peaks (Fig. 1 and Fig. S1, blue lines) are considerably shifted to more positive potentials. The effect of the HER or solvent co-reduction on the voltammetric profiles of Cu(111) is considerably stronger than on Cu(100), which surface remains less altered by the selected potential limits. This shows that Cu(111) is highly sensitive to undergo surface changes under reduction conditions, as we have discussed in our previous report.[23] The surface restructuring also takes places in the absence of CO, being an intrinsic behavior of the (111) orientation (Fig. S1B).

Importantly, the charge under the voltammetric peak remains constant with the pH on both Cu(100) and Cu(111), and the presence of CO does not modify this value. The charge value approaches to 45-55μC $cm^{-2}$ on Cu(100), and to 50-60 μC$cm^{-2}$ on Cu(111), in agreement with previous works (Fig. S2).[30,42] Given that the ideal one-electron surface charge areas of Cu(111) and Cu(100) are, respectively, 284 and 247 μC $cm^{-2}$,[43,44] the previous calculated charges from the CVs are considerably low, especially if we assume that the adsorption of phosphate species involve the transfer of more than one single electron. The calculated charges through integrated voltammetric peaks suggest that there are uncertainties in the estimation of the real surface coverage through charge coverages on the surface.

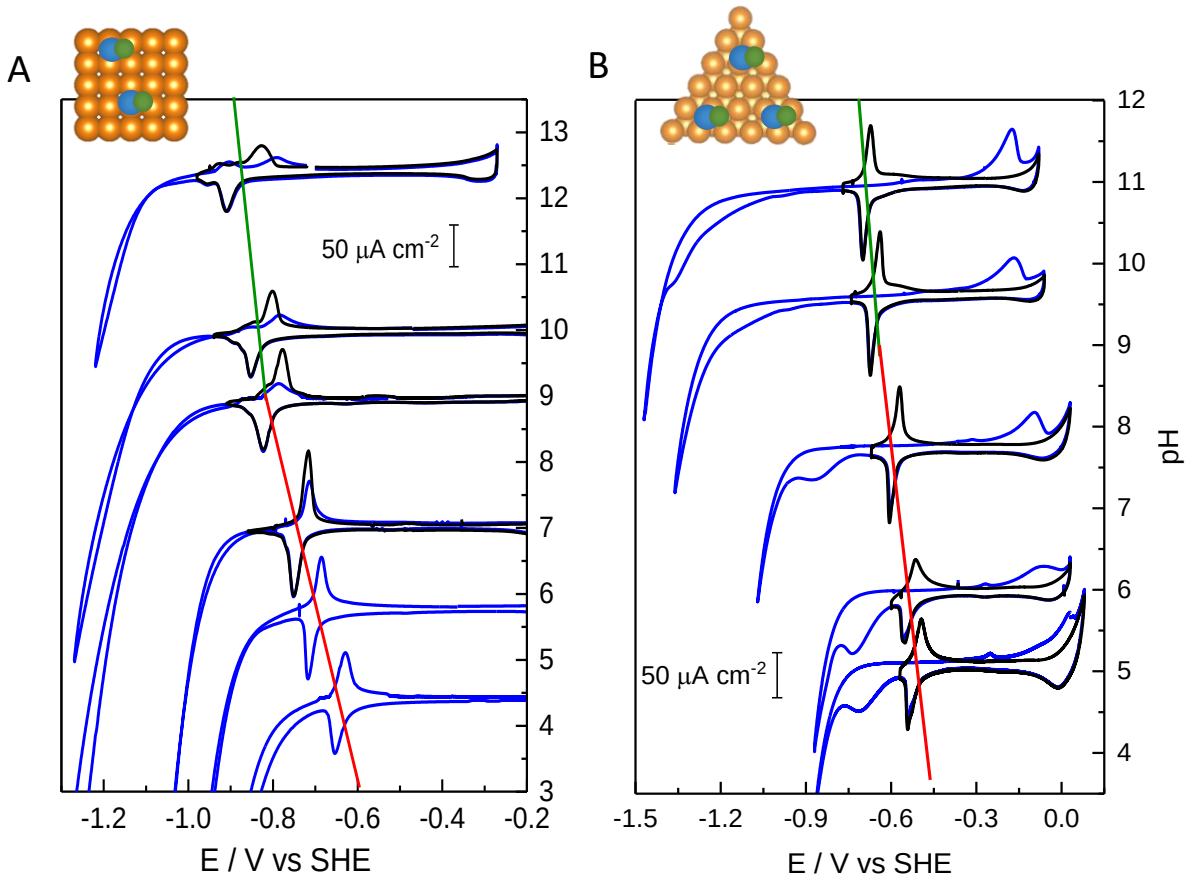


Figure 1: Cyclic voltammograms of the Cu(hkl) | CO-saturated 0.1 M phosphate buffer interface as a function of the pH (right axis). Scan rate: 50mV/s. A) Cu(100), B) Cu(111). Red and green solid lines cross the CO peak at each pH. Blue lines and black lines are consecutive cycles recorded without breaking the hanging meniscus configuration. Black curves show the CVs recorded in short potential windows while, in the blue curves (long potential windows), the cathodic potential limit was enlarged towards the HER and the CO reduction.

To analyze in detail the effect of the pH on the onset potential of CO adsorption on Cu-single crystalline electrodes, we have plotted the potential average value between anodic peak ($E_a$) and cathodic peak($E_c$) of the CO-displacement voltammetric feature, i.e. ($\frac{Ea+Ec}{2}$) (Fig. 2A). We have

extracted the CO-peak potential values from the voltammetric data recorded at narrow potential windows (Fig. 1, black lines). The averaged potential peak value is assumed to be close to the equilibrium potential of the competing adsorption/desorption reaction between the phosphate species and the CO on both Cu surfaces (Eq 1 and Fig. S3).[30] The potential peak shift with the pH is about 36 mV $pH^{-1}$ on Cu(111) (Fig. 2A, black circles) and 33 mV $pH^{-1}$ on Cu(100) (Fig. 2A, blue squares).[30] In contrast, in alkaline media this trend changes, and the potential shift with the pH is more flattered on both surfaces. The obtained slope is about 15 mV per pH unity on Cu(100) and 21mV on Cu(111). Figure 2A clearly shows that CO-peak values on Cu(111) appears allocated at more positive potential values than on Cu(100), which is likely due to phosphate poisons less strong <111> facets than <100> facets.

To get a deeper insight into the phosphate poisoning effect, we have compared the CVs of both Cu(100) and Cu(111) in phosphate blank solutions at high pH with the CVs obtained in the presence of CO (Fig. 2B). Here, we have plotted the cathodic potential peak of both Cu(111) and Cu(100) from either blank phosphate solutions or solutions with CO (Fig 2C). We have selected the potential of the cathodic peak ($E_c$) because the blank CVs of Cu(100) loses symmetry in the anodic scan at pH < 12 due to overlapping with the HER at these pH (See Fig. S1A). Red symbols represent the phosphate peak in the blank solutions, while black symbols are the CO peaks obtained from the CO-saturated solutions (Fig. 2C). The potential difference between phosphate and CO peaks on Cu(111) is small, about 30mV, supporting that CO weakly adsorbs on this surface. In contrast, on Cu(100), this potential difference between phosphate and CO peaks is considerable higher, about 100 mV (Fig. 2B and C). This suggests that CO possibly adsorbs stronger on Cu(100) than on Cu(111). Despite that, the CO peaks appear at more negative potential values on Cu(100)

than on Cu(111), which indicates that the strong adsorption of phosphate on both Cu(100) and Cu(111) is the main parameter controlling the potential windows for CO adsorption on the surface.

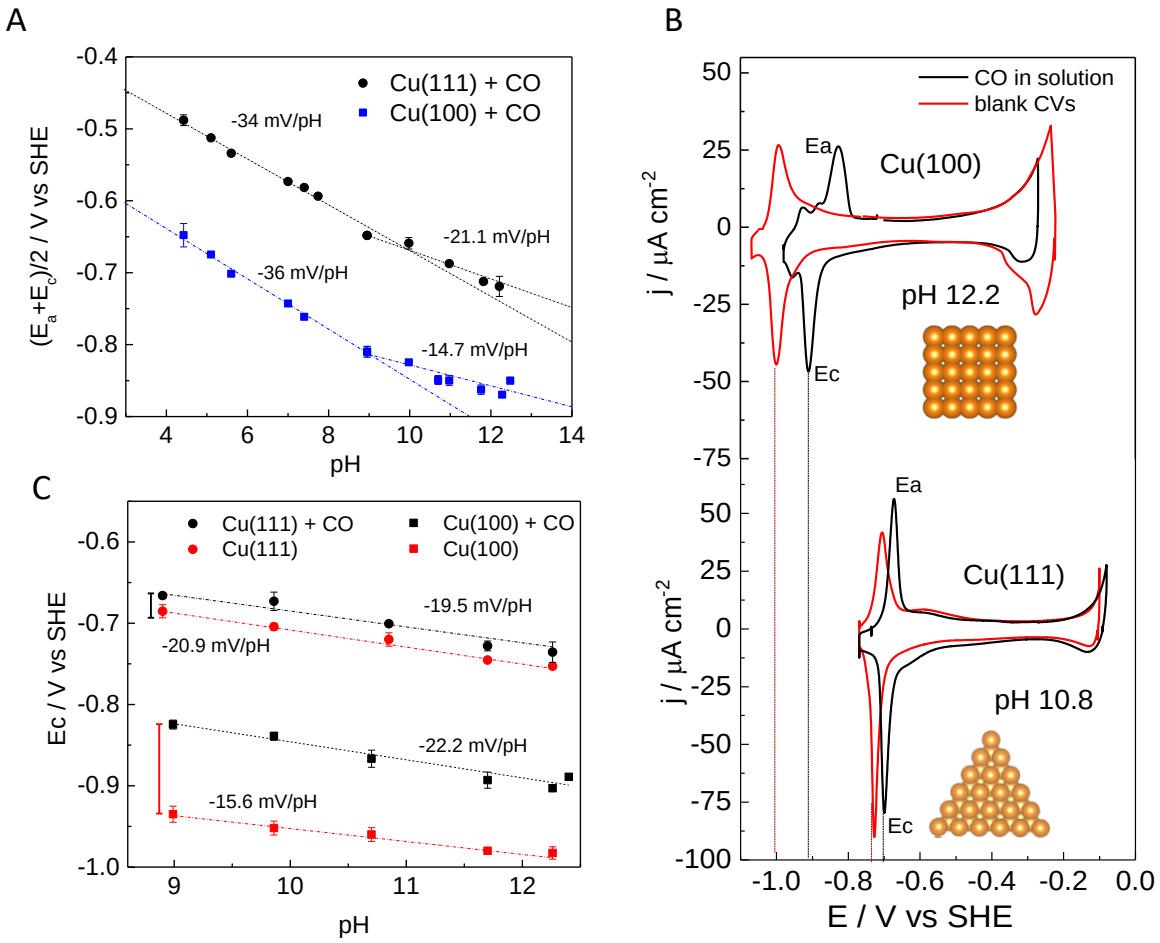


Figure 2: A) Plot of $(E_c-E_a)/2$ vs pH of both Cu(100) (blue squares) and Cu(111) (black circles) in phosphate buffer solutions and in presence of CO. B) C) Cyclic voltammograms of both Cu(111) and Cu(100) in red line) 0.1 M alkaline phosphate buffer solution, black line) same solution with CO. 50mV/s. C) Plot of the cathodic potential peak ($E_c$) vs pH in 0.1 M phosphate buffer solutions with CO (black symbols) and without CO (red symbols).

Experimental results were assessed under the lights of simulations of the interfacial region of Cu and the aqueous electrolyte, employing AIMD simulations of explicit electrolyte in contact with the surfaces. In the simulations of both Cu(100) and Cu(111) | phosphate electrolyte interface, the Cu surfaces were covered with H* and OH* from zero up to half coverage. Additionally, the electrolyte was simulated with single $H_xPO_4$ anions, as well as with (OC)CO* and (OC)COH* species adsorbed at the surface. The parentheses denote whether the adsorbed CO specie is a dimer or monomer, *i.e.* on Cu(100) the dimers are stable, whereas on Cu(111) the monomer is the stable CO specie. The adsorbates included in AIMD simulations are summarized in the S.I. (Table S1). In order to apply the generalized computational hydrogen electrode (GCHE) scheme, the work function and energy for each state from the AIMD simulations are saved. The GCHE scheme enables the explicit simulations of the interface phase diagrams, as the potential and the chemical potential of the ions are expressed by the work function and corresponding energetics. At each integer of pH, the most stable surface configurations were obtained by binning the work function in bins of a size of 0.02 eV. All GCHE energy states within each bin were Boltzmann-weighted.

In Fig. 3A) and B), the coverage on Cu(100) (Fig. 3A) and on Cu(111) (Fig. 3B) of adsorbates are presented as a contour plot relative to the standard hydrogen electrode ($U_{SHE}$) potential and the pH. Each bin with a coverage above 0.1 monolayer of one of the (OC)CO*, (OC)COH*, and $H_xPO_4$ adsorbates has been assigned with the respective color of the legend, whereas the varying coverages of H* and OH* are assigned with the color bar. The methodology of including phosphate anions in the GCHE has previously been applied for Cu[22] and is further elaborated in the S.I (Fig. S4 and S5). In summary, the methodology accounts for the phosphate reference to change concurrently with changes in pH, *i.e.* the phosphate species in the bulk electrolyte become less protonated with increasing pH. The change in phosphate reference is depicted in the S.I. (Fig. S5).

The results from Fig. 3A) and B) show that in acidic and neutral pH, the Cu facets are covered with phosphate species up to high overpotentials, whereas at more alkaline conditions, the phosphate anions become unstable, leading to the CO* being adsorbed at an earlier potential. As the coverages of adsorbates change, a current ($j$) is generated. The resulting current density is derived by the gradients of the Pourbaix diagrams, as the derivative of the Boltzmann-weighted energetics corresponds to the isotherm from the surface. Differentiating once again and multiplying with a chosen scan rate yields the resulting current density from interchanging adsorbates[45], hence this method of deriving current densities does not asses kinetics of surface reactions. The current density is per definition symmetric cathodically and anodically, hence the current densities are independent of the scan direction.

Fig. 3C) and D) shows the resulting current densities from interchanging adsorbates for Cu(100) and Cu(111), respectively. When revisiting Fig. 3A) and B), it is possible to assign the current density to the corresponding interchange of adsorbates. The lower blue line with the negative slope per pH unity arises from the adsorption of $H^*$, allowing hydrogen to evolve. In addition, the interchange from 4 $OH^*$ to an adsorbed phosphate anion results in the other blue region. The current density in the deep red region arises from the adsorbate interchange of phosphate anion and CO species.

To investigate the shift in the CO peak, a Gaussian distribution is fitted to the current density, arising from the interchange of phosphate anion and CO specie, at every pH unity. The mean of each Gaussian distribution is plotted in Fig. 3 as well. The potential peak shift follows a linear trend with the pH, which resembles the experimental observed trends, *i.e.* as the pH increases, the CO surface poisoning shifts linearly to higher overpotentials, with a slope of 41 mV per pH unity. In contrast, at alkaline pH values, the potential peak shift with the pH is smaller, with a slope of

18 mV per pH unity for Cu(100) and 24 mV per pH unity for Cu(111), respectively To rationalize the results from Fig. 3), a set of possible reactions of interchanging the phosphate adsorbates with CO species are proposed, based on the general reaction (1). The reactions are summarized in Table 1. From Fig. 3), the dominating CO* species differ on the two Cu facets, *i.e*. OCCOH* is adsorbed on Cu(100) and CO* is adsorbed on Cu(111). This highlights that, beyond the fact that CO poisoning shows different strength and potential dependence in each orientation, the structure sensitivity in the intermediate formation may steer the different selectivity observed on both facets at sufficient applied potential. In addition to different CO species, the dominating phosphate anion species depend on the Cu facet as well, *i.e.* on the Cu(100) facet, $HPO_4$* is the dominating phosphate specie, whereas the adsorbed phosphate species changes on Cu(111) from $HPO_4^*$ to $PO_4$* towards more neutral pHs (Fig. S6). As pH is increased, the adsorption occurring on the surface evolves from Eq. (1) towards Eq. (4), with Eq. (2) and Eq. (3) being the most predominant reactions in the pH range of the experiment. The corresponding slopes are derived from the Nernst equation,[38] in the base-10 log form, at room temperature.

| | | | Slope / [mV/pH] |
|---|---|---|---|
| Cu(100) | 1 | $HPO_4^* + 2\,CO + 3\,H^+ + 3\,e^- \rightleftharpoons H_3PO_4\,(aq) + OCCOH^*$ | -59.2 |
| | 2 | $HPO_4^* + 2\,CO + 2\,H^+ + 3\,e^- \rightleftharpoons H_2PO_4^-\,(aq) + OCCOH^*$ | -39.5 |
| | 3 | $HPO_4^* + 2\,CO + H^+ + 3\,e^- \rightleftharpoons HPO_4^{2-}\,(aq) + OCCOH^*$ | -19.7 |
| | 4 | $HPO_4^* + 2\,CO + 3\,e^- \rightleftharpoons PO_4^{3-}\,(aq) + OCCOH^*$ | 0 |
| Cu(111) | 1 | $HPO_4^* + CO + 2\,H^+ + 2\,e^- \rightleftharpoons H_3PO_4\,(aq) + CO^*$ | -59.2 |
| | 2 | $PO_4^* + CO + 2\,H^+ + 3\,e^- \rightleftharpoons H_2PO_4^-\,(aq) + CO^*$ | -39.5 |

| | | |
|---|---|---|
| 3 | $PO_4^* + CO + H^+ + 3\,e^- \rightleftharpoons HPO_4^{2-}\,(aq) + CO^*$ | -19.7 |
| 4 | $PO_4^* + CO + \,3\,e^- \rightleftharpoons PO_4^{3-}\,(aq) + CO^*$ | 0 |

Table 1: A proposed set of equations of the adsorbate interchange between the CO species and phosphate anions. The slopes are determined according to the Nernst equation, in the base-10 log form, at room temperature.

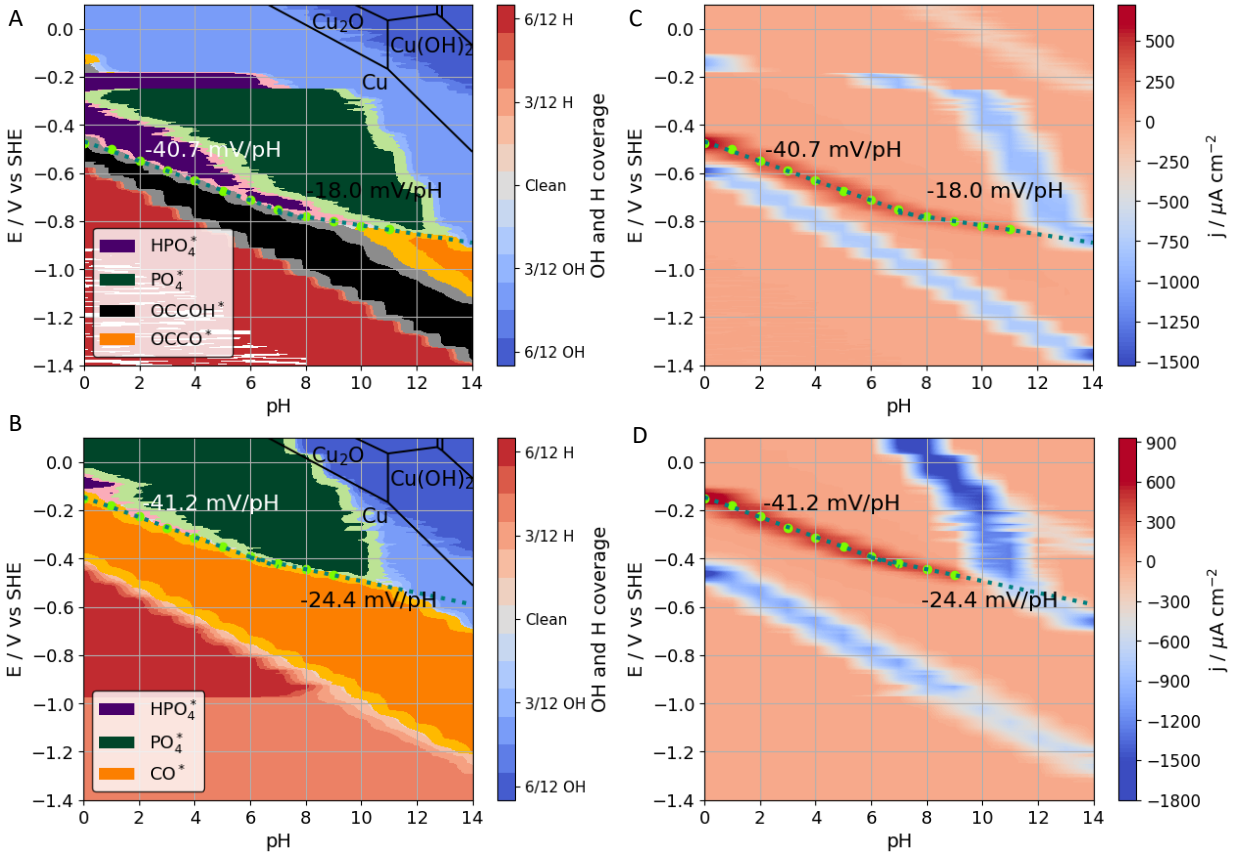


Figure 3: A and B show the interface Pourbaix diagrams of the most stable species on A) Cu(100) and B) Cu(111) as a function of pH and potential, calculated by Boltzmann-weighted binning of the energetics obtained by the GCHE scheme. The black lines show the stable phases of Cu as a function of pH and potential at 25°C. Data is adapted from [46]. C) and D) represent the current density for Cu(100) and Cu(111), respectively, as a function of pH and potential as derived by the

gradient of the Pourbaix diagram. The pale areas indicate a constant charge on the surface, whereas the blue and red areas indicate current arising when coverages of adsorbates change. The dotted lines are the means of the Gaussian distributions fitted to the current density at each unity of pH.

To better compare experimental results with simulations, we have in Fig. 4 plotted the values of the averaged CO-potential peaks, $\left(\frac{Ea+Ec}{2}\right)$, of Cu(100) and Cu(111) from the CVs in Fig. 2, with the CO peak values extrapolated from simulations (Fig. 3). In both experiments and simulations, the CO adsorption on Cu(111) occurs at more positive potentials because of the weak anion binding on Cu(111). The binding strengths of phosphate anions and CO species are shown in the S.I. (Fig. S7). The figure shows a clear tendency of Cu(100) binding adsorbates significantly stronger than Cu(111). The experimental measurements show similar behavior in the difference between the peak shifts. However, when compared to the experimental results, the peak potentials for Cu(111) are shifted quite considerably to more positive values. This discrepancy might be due to different uncertainties, arising from the simulation model, *e.g.* the entropy of the adsorbed species at the surface is approximated to 0. Nonetheless, the main limitations of the simulation's validity arise from the limited number of included possible simulated interface structures and the corresponding sampled energetics. These limitations impose uncertainties on the coverages of the adsorbates, resulting in the uncertainties in the corresponding charge transfer and onset potentials.

Noteworthy, the slopes of the linear trends for the CO-displacement peak originates from the anion reference and model itself, which omit the uncertainties from the simulations of specific coverages and energetics. The robustness by ± 0.5 eV of the anion reference is depicted in Fig. S8. Despite the uncertainties with coverage and the phosphate anion reference, the overall phosphate

electrolyte tendencies align with the experimental results obtained, and by previous observations made by Hori et al.[30,36] and in simulations.[22]

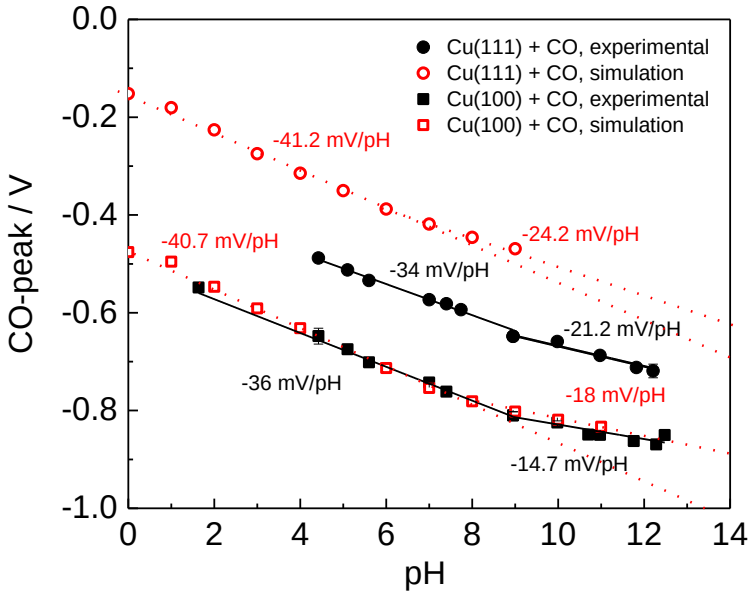


Figure 4: Plot of the CO-peaks as a function of the pH for black solid symbols) results obtained experimentally, red open symbols) from simulations of the Cu(hkl) | CO-saturated 0.1 M phosphate solution.

In our previous report,[22] we performed AIMD simulations to study the structure of the electrolyte interface Cu(100) for CO reduction, in contact with three different electrolytes: neutral bicarbonate solutions, neutral phosphate buffer solution and alkaline media.[22,47,48] We observed that, in electrolytes containing anions that specifically adsorb on Cu(100), such as bicarbonate or phosphate anions, the anion poisoning the surface controlled the potential range at which the main CO* intermediate was stabilized. We suggested that the onset potential for the formation of the main products, i.e. $C_2H_4$ on Cu(100), in neutral buffer solutions, is clearly limited by the anion

blocking the surface and not only affected by the solution pH.[12] Here, we show that both experiments and simulations underline that the CO poisoning on Cu single-crystalline electrodes is controlled by the specific properties of the Cu(hkl) | electrolyte interface.

Additionally, our simulations in this work suggest that PO4* is the main adsorbed species on Cu(111), even at acidic pHs, while on Cu(100) we observe the protonated HPO4*. Hori et al.,[30] as well as other authors for diverse reactions,[49,50] postulated that the pKa of the adsorbed anions in the metal-electrolyte interface is considerably lower compared to the pKa in the solution. On Cu(111), the drop of the pKa must be particularly pronounced, since its tendency is to stabilize the deprotonated PO4* at low pH. Remarkably, the efficiency of the CO reduction on Cu and in phosphate neutral media, is considerably affected by competition with the hydrogen evolution reaction (HER).[51] In contrast, the HER on Cu is better suppressed in other neutral electrolytes containing, e.g., bicarbonate, chloride or sulphate solutions, in which the product selectivity towards multi-carbon products is significantly improved.[51] The strongest acidity gained by the phosphate anions (Table 1) at the electrode surface could also contribute to enhance the selectivity towards the HER, which makes the neutral phosphate buffer electrolyte a poor candidate for the CO reduction reaction.

**Conclusions**

Herein we aimed to provide a detailed description of the structure of the interface between Cu(111) and Cu(100) | phosphate buffer solutions in presence of CO. The interfacial properties of the Cu(hkl)-electrolyte interface were assessed by combining voltammetric CO-displacement measurements and ab-initio simulations of the Cu single-crystalline electrodes-electrolyte interfaces. Good alignment was found between experiments and simulations, from which we showed that:

a) CO adsorbs on the surface in the potential region close to the desorption of phosphate species anions from the electrolyte. Theoretical calculations suggest that the predominant adsorbed specie is $HPO_4^*$ on Cu(100), while it is $PO_4^*$on Cu(111).

b) The adsorption of CO on Cu(111) takes place at less negative potential values than on Cu(100) due to the lower binding energy of phosphate species on Cu(111).

c) CO adsorption is stronger on Cu(100) than on Cu(111), shown by the more pronounced shift of the phosphate peaks CVs by CO on Cu(100) than on Cu(111), despite the fact that the phosphate adsorption on Cu(100) is stronger.

d) Experiments and simulations evidenced that the onset potential at which CO adsorbs on the surface is controlled by the properties of the Cu(hkl)-electrolyte interface, and particularly limited by the anion blocking the surface.

This work highlights the importance of combining cyclic voltammetry under potential control with theoretical calculations to find the relations between interfacial properties of Cu electrodes and electrocatalytic CO reduction. Future work should be encouraged to elucidate and rationalize how specific electrolyte interactions and solvent reaction affect the surface structure stability of Cu-single crystalline surfaces under different potential conditions, as well as its influence on the CORR performance.

AUTHOR INFORMATION

*Corresponding author:

E-mail: maria.escudero@chem.ku.dk

E-mail: alexander@chem.ku.dk

ORCID

Paula Sebastián-Pascual: 0000-0001-7985-0750

Amanda Schramm Petersen: 0000-0001-8818-0031

Alexander Bagger: 0000-0002-6394-029X

Jan Rossmeisl: 0000-0001-7749-6567

María Escudero-Escribano: 0000-0002-6432-3015

**Notes**

The authors declare no competing financial interest.

ASSOCIATED CONTENT

Detailed description of experimental details and computational details are included in the supporting information. Blank cyclic voltammograms of both Cu(111) and Cu(100) in phosphate buffer solutions, charge values and additional analysis of phosphate and CO peaks on both Cu facets are also included. The supporting information also contains the simulations of the Cu(111) and Cu(100) interfaces in contact with blank solutions.

Atomic structures and interface models, together with databases and analysis scripts, are available on the webpage: https://nano.ku.dk/english/research/theoretical-electrocatalysis/katladb/ph-and-anion-effects-on-cu-phosphate-interfaces-for-co-electroreduction/.

ACKNOWLEDGMENT

MEE and PSP gratefully acknowledge the Villum Foundation for financial support through a Villum Young Investigator Grant (project number: 19142). We acknowledge support from the Villum Center for the Science of Sustainable Fuels and Chemicals (V-sustain, grant number 9455) and the Danish National Research Foundation Center for High Entropy Alloy Catalysis (CHEAC, DNRF-149).

**References**

(1) Eisenberg, R.; Gray, H. B.; Crabtree, G. W. Addressing the Challenge of Carbon-Free Energy. *Proc. Natl. Acad. Sci. U. S. A.* **2020**, *117* (23), 12543–12549. https://doi.org/10.1073/pnas.1821674116.

(2) De Luna, P.; Hahn, C.; Higgins, D.; Jaffer, S. A.; Jaramillo, T. F.; Sargent, E. H. What Would It Take for Renewably Powered Electrosynthesis to Displace Petrochemical Processes? *Science (80-. ).* **2019**, *364* (6438), eaav3506. https://doi.org/10.1126/science.aav3506.

(3) Eisenberg, R. Addressing the Challenge of Carbon-Free Energy. *ACS Energy Lett.* **2018**, *3* (7), 1521–1522. https://doi.org/https://doi.org/10.1021/acsenergylett.8b00889.

(4) Nitopi, S. A.; Bertheussen, E.; Scott, S. B.; Liu, X.; Albert, K.; Horch, S.; Seger, B.; Stephens, I. E. L.; Chan, K.; Nørskov, J. K.; Jaramillo, T. F.; Chorkendorff, I. Progress and Perspectives of Electrochemical CO2 Reduction on Copper in Aqueous Electrolyte. *Chem. Rev.* **2019**, *119* (12), 7610–7672. https://doi.org/10.1021/acs.chemrev.8b00705.

(5) Gao, D.; Arán-Ais, R. M.; Jeon, H. S.; Roldan Cuenya, B. Rational Catalyst and Electrolyte Design for CO2 Electroreduction towards Multicarbon Products. *Nat. Catal.* **2019**, *2* (3), 198–210. https://doi.org/10.1038/s41929-019-0235-5.

(6) Sebastián-Pascual, P.; Mezzavilla, S.; Stephens, I. E. L.; Escudero-Escribano, M. Structure-Sensitivity and Electrolyte Effects in CO2 Electroreduction: From Model Studies to Applications. *ChemCatChem* **2019**, *21* (0), 3626–3645. https://doi.org/10.1002/cctc.201900552.

(7) Kuhl, K. P.; Cave, E. R.; Abram, D. N.; Jaramillo, T. F. New Insights into the Electrochemical Reduction of Carbon Dioxide on Metallic Copper Surfaces. *Energy Environ. Sci.* **2012**, *5* (5), 7050–7059. https://doi.org/10.1039/c2ee21234j.

(8) Bagger, A.; Ju, W.; Varela, A. S.; Strasser, P.; Rossmeisl, J. Electrochemical CO2 Reduction: A Classification Problem. *ChemPhysChem* **2017**, *18* (22), 3266–3273. https://doi.org/10.1002/cphc.201700736.

(9) Peterson, A. A.; Abild-Pedersen, F.; Studt, F.; Rossmeisl, J.; Nørskov, J. K. How Copper Catalyzes the Electroreduction of Carbon Dioxide into Hydrocarbon Fuels. *Energy Environ. Sci.* **2010**, *3* (9), 1311–1315. https://doi.org/10.1039/c0ee00071j.

(10) Hori, Y.; Murata, A.; Takahashi, R.; Suzuki, S. Electroreduction of CO to CH4 and C2H4 at a Copper Electrode in Aqueous Solutions at Ambient Temperature and Pressure. *J. Am. Chem. Soc.* **1987**, *109* (16), 5022–5023. https://doi.org/10.1021/ja00250a044.

(11) Hori, Y.; Murata, A.; Yoshinami, Y. Adsorption of Carbon Monoxide, Intermediately Formed in Electrochemical Reduction of Carbon Dioxide, at a Copper Electrode. *J. Chem.*

*Soc., Faraday Trans.* **1991**, *87* (Copyright (C) 2011 American Chemical Society (ACS). All Rights Reserved.), 125–128. https://doi.org/10.1039/ft9918700125.

(12) Schouten, K. J. P.; Qin, Z.; Gallent, E. P.; Koper, M. T. M. Two Pathways for the Formation of Ethylene in CO Reduction on Single-Crystal Copper Electrodes. *J. Am. Chem. Soc.* **2012**, *134* (24), 9864–9867. https://doi.org/10.1021/ja302668n.

(13) Schouten, K. J. P.; Pérez-Gallent, E.; Koper, M. T. M. Structure Sensitivity of the Electrochemical Reduction of Carbon Monoxide on Copper Single Crystals. *ACS Catal.* **2013**, *3* (6), 1292–1295. https://doi.org/10.1021/cs4002404.

(14) Birdja, Y. Y.; Pérez-Gallent, E.; Figueiredo, M. C.; Göttle, A. J.; Calle-Vallejo, F.; Koper, M. T. M. Advances and Challenges in Understanding the Electrocatalytic Conversion of Carbon Dioxide to Fuels. *Nat. Energy* **2019**, *4* (9), 732–745. https://doi.org/10.1038/s41560-019-0450-y.

(15) Rendón-Calle, A.; Builes, S.; Calle-Vallejo, F. A Brief Review of the Computational Modeling of CO2 Electroreduction on Cu Electrodes. *Curr. Opin. Electrochem.* **2018**, *9*, 158–165. https://doi.org/10.1016/J.COELEC.2018.03.012.

(16) Hori, Y.; Takahashi, R.; Yoshinami, Y.; Murata, A. Electrochemical Reduction of CO at a Copper Electrode. *J. Phys. Chem. B* **1997**, *101* (36), 7075–7081. https://doi.org/10.1021/jp970284i.

(17) Hahn, C.; Hatsukade, T.; Kim, Y.-G.; Vailionis, A.; Baricuatro, J. H.; Higgins, D. C.; Nitopi, S. A.; Soriaga, M. P.; Jaramillo, T. F. Engineering Cu Surfaces for the Electrocatalytic Conversion of CO2 : Controlling Selectivity toward Oxygenates and

Hydrocarbons. *Proc. Natl. Acad. Sci.* **2017**, *114* (23), 5918–5923. https://doi.org/10.1073/pnas.1618935114.

(18) Pérez-Gallent, E.; Marcandalli, G.; Figueiredo, M. C.; Calle-Vallejo, F.; Koper, M. T. M. Structure- and Potential-Dependent Cation Effects on CO Reduction at Copper Single-Crystal Electrodes. *J. Am. Chem. Soc.* **2017**, *139* (45), 16412–16419. https://doi.org/10.1021/jacs.7b10142.

(19) Huang, Y.; Handoko, A. D.; Hirunsit, P.; Yeo, B. S. Electrochemical Reduction of CO2 Using Copper Single-Crystal Surfaces: Effects of CO* Coverage on the Selective Formation of Ethylene. *ACS Catal.* **2017**, *7* (3), 1749–1756. https://doi.org/10.1021/acscatal.6b03147.

(20) Arán-Ais, R. M.; Scholten, F.; Kunze, S.; Rizo, R.; Roldan Cuenya, B. The Role of in Situ Generated Morphological Motifs and Cu(i) Species in C2+ Product Selectivity during CO2 Pulsed Electroreduction. *Nat. Energy* **2020**, *5*, 317–325. https://doi.org/10.1038/s41560-020-0594-9.

(21) Tiwari, A.; Heenen, H. H.; Bjørnlund, A. S.; Maagaard, T.; Cho, E.; Chorkendorff, I.; Kristoffersen, H. H.; Chan, K.; Horch, S. Fingerprint Voltammograms of Copper Single Crystals under Alkaline Conditions: A Fundamental Mechanistic Analysis. *J. Phys. Chem. Lett.* **2020**, *11* (4), 1450–1455. https://doi.org/10.1021/acs.jpclett.9b03728.

(22) Bagger, A.; Arnarson, L.; Hansen, M. H.; Spohr, E.; Rossmeisl, J. Electrochemical CO Reduction: A Property of the Electrochemical Interface. *J. Am. Chem. Soc.* **2019**, *141* (4), 1506–1514. https://doi.org/10.1021/jacs.8b08839.

(23) Sebastián-Pascual, P.; Escudero-Escribano, M. Addressing the Interfacial Properties for CO Electroreduction on Cu with Cyclic Voltammetry. *ACS Energy Lett.* **2020**, *5* (1), 130–135. https://doi.org/10.1021/acsenergylett.9b02456.

(24) Le Duff, C. S.; Lawrence, M. J.; Rodriguez, P. Role of the Adsorbed Oxygen Species in the Selective Electrochemical Reduction of CO2 to Alcohols and Carbonyls on Copper Electrodes. *Angew. Chemie - Int. Ed.* **2017**, *56* (42), 12919–12924. https://doi.org/10.1002/anie.201706463.

(25) Varela, A. S.; Kroschel, M.; Reier, T.; Strasser, P. Controlling the Selectivity of CO2 Electroreduction on Copper: The Effect of the Electrolyte Concentration and the Importance of the Local PH. *Catal. Today* **2016**, *260*, 8–13. https://doi.org/10.1016/j.cattod.2015.06.009.

(26) Sebastian-Pascual, P.; Sarabia, F. J.; Climent, V.; Feliu, J. M.; Escudero-Escribano, M. Elucidating the Structure of the Cu-Alkaline Electrochemical Interface with the Laser-Induced Jump Temperature Method. *J. Phys. Chem. C* **2020**, *124* (42), 23253–23259. https://doi.org/10.1021/acs.jpcc.0c07821.

(27) Stenlid, J. H.; Dos Santos, E. C.; Bagger, A.; Johansson, A. J.; Rossmeisl, J.; Pettersson, L. G. M. Electrochemical Interface during Corrosion of Copper in Anoxic Sulfide-Containing Groundwater—A Computational Study. *J. Phys. Chem. C* **2020**, *124* (1), 469–481. https://doi.org/10.1021/acs.jpcc.9b08657.

(28) Ooka, H.; Figueiredo, M. C.; Koper, M. T. M. Competition between Hydrogen Evolution and Carbon Dioxide Reduction on Copper Electrodes in Mildly Acidic Media. *Langmuir*

**2017**, *33* (37), 9307–9313. https://doi.org/10.1021/acs.langmuir.7b00696.

(29) Varela, A. S. The Importance of PH in Controlling the Selectivity of the Electrochemical CO2 Reduction. *Curr. Opin. Green Sustain. Chem.* **2020**, 100371. https://doi.org/https://doi.org/10.1016/j.cogsc.2020.100371.

(30) Koga, O.; Watanabe, Y.; Tanizaki, M.; Hori, Y. Specific Adsorption of Anions on a Copper (100) Single Crystal Electrode Studied by Charge Displacement by CO Adsorption and Infrared Spectroscopy. *Electrochim. Acta* **2001**, *46* (20–21), 3083–3090. https://doi.org/10.1016/S0013-4686(01)00599-0.

(31) Ovalle, V. J.; Waegele, M. M. Impact of Electrolyte Anions on the Adsorption of CO on Cu Electrodes. *J. Phys. Chem. C* **2020**, *124* (27), 14713–14721. https://doi.org/10.1021/acs.jpcc.0c04037.

(32) Jensen, K. D.; Tymoczko, J.; Rossmeisl, J.; Bandarenka, A. S.; Chorkendorff, I.; Escudero-Escribano, M.; Stephens, I. E. L. Elucidation of the Oxygen Reduction Volcano in Alkaline Media Using a Copper–Platinum(111) Alloy. *Angew. Chemie - Int. Ed.* **2018**, *57* (11), 2800–2805. https://doi.org/10.1002/anie.201711858.

(33) Dong, J.-C.; Zhang, X.-G.; Briega-Martos, V.; Jin, X.; Yang, J.; Chen, S.; Yang, Z.-L.; Wu, D.-Y.; Feliu, J. M.; Williams, C. T.; Tian, Z.-Q.; Li, J.-F. In Situ Raman Spectroscopic Evidence for Oxygen Reduction Reaction Intermediates at Platinum Single-Crystal Surfaces. *Nat. Energy* **2019**, *4* (1), 60–67. https://doi.org/10.1038/s41560-018-0292-z.

(34) Gómez-Marín, A. M.; Rizo, R.; Feliu, J. M. Oxygen Reduction Reaction at Pt Single

Crystals: A Critical Overview. *Catalysis Science and Technology*. The Royal Society of Chemistry 2014, pp 1685–1698. https://doi.org/10.1039/c3cy01049j.

(35) Strmcnik, D.; Escudero-Escribano, M.; Kodama, K.; Stamenkovic, V. R.; Cuesta, A.; Marković, N. M. Enhanced Electrocatalysis of the Oxygen Reduction Reaction Based on Patterning of Platinum Surfaces with Cyanide. *Nat. Chem.* **2010**, *2*, 880–885. https://doi.org/https://doi.org/10.1038/nchem.771.

(36) Hori, Y.; Koga, O.; Watanabe, Y.; Matsuo, T. FTIR Measurements of Charge Displacement Adsorption of CO on Poly- and Single Crystal (100) of Cu Electrodes. *Electrochim. Acta* **1998**, *44* (8–9), 1389–1395. https://doi.org/10.1016/S0013-4686(98)00261-8.

(37) Koga, O.; Matsuo, T.; Hoshi, N.; Hori, Y. Charge Displacement Adsorption of Carbon Monoxide on [110] Zone Copper Single Crystal Electrodes in Relation with PZC. *Electrochim. Acta* **1998**, *44* (6–7), 903–907. https://doi.org/10.1016/S0013-4686(98)00193-5.

(38) Bard, A. J.; Faulkner, L. R. Electrochemical Methods : Fundamentals and Applications / 2. Potentials and Thermodynamics of Cells. **2001**, 44–86.

(39) Kim, Y.-G.; Javier, A.; Baricuatro, J. H.; Torelli, D.; Cummins, K. D.; Tsang, C. F.; Hemminger, J. C.; Soriaga, M. P. Surface Reconstruction of Pure-Cu Single-Crystal Electrodes under CO-Reduction Potentials in Alkaline Solutions: A Study by Seriatim ECSTM-DEMS. *J. Electroanal. Chem.* **2016**, *780*, 290–295. https://doi.org/10.1016/J.JELECHEM.2016.09.029.

(40) Matsushima, H.; Taranovskyy, A.; Haak, C.; Gründer, Y.; Magnussen, O. M. Reconstruction of Cu(100) Electrode Surfaces during Hydrogen Evolution. *J. Am. Chem. Soc.* **2009**, *131* (30), 10362–10363. https://doi.org/10.1021/ja904033t.

(41) Kim, Y. G.; Baricuatro, J. H.; Javier, A.; Gregoire, J. M.; Soriaga, M. P. The Evolution of the Polycrystalline Copper Surface, First to Cu(111) and Then to Cu(100), at a Fixed CO2RR Potential: A Study by Operando EC-STM. *Langmuir* **2014**, *30* (50), 15053–15056. https://doi.org/10.1021/la504445g.

(42) Grunder, Y.; Beane, J.; Kolodziej, A.; Lucas, C. A.; Rodriguez, P. Potential Dependent Structure and Stability of Cu(111) in Neutral Phosphate Electrolyte. *Surfaces* **2019**, *2* (1), 145–158. https://doi.org/10.3390/surfaces2010012.

(43) Brisard, G. M.; Zenati, E.; Gasteiger, H. A.; Marković, N. M.; Ross, P. N. Underpotential Deposition of Lead on Cu(100) in the Presence of Chloride: Ex-Situ Low-Energy Electron Diffraction, Auger Electron Spectroscopy, and Electrochemical Studies. *Langmuir* **1997**, *13* (8), 2390–2397. https://doi.org/10.1021/la960999x.

(44) Brisard, G. M.; Zenati, E.; Gasteiger, H. A.; Markovic, N.; Ross, P. N. Underpotential Deposition of Lead on Copper(111): A Study Using a Single-Crystal Rotating Ring Disk Electrode and Ex Situ Low-Energy Electron Diffraction and Scanning Tunneling Microscopy. *Langmuir* **1995**, *11* (6), 2221–2230. https://doi.org/10.1021/la00006a060.

(45) Rossmeisl, J.; Jensen, K. D.; Petersen, A. S.; Arnarson, L.; Bagger, A.; Escudero-Escribano, M. Realistic Cyclic Voltammograms from Ab Initio Simulations in Alkaline and Acidic Electrolytes. *J. Phys. Chem. C* **2020**, *124* (37), 20055–20065.

https://doi.org/10.1021/acs.jpcc.0c04367.

(46) Beverskog, B.; Puigdomenech, I. Revised Pourbaix Diagrams for Copper at 25 to 300°C. *J. Electrochem. Soc.* **1997**, *144* (10), 3476–3483. https://doi.org/10.1149/1.1838036.

(47) Bagger, A.; Arán-Ais, R. M.; Halldin Stenlid, J.; dos Santos, E.; Arnarson, L.; Degn Jensen, K.; Escudero-Escribano, M.; Roldan Cuanya, B.; Rossmeisl, J. Ab Initio Cyclic Voltammetry on Cu(111), Cu(100) and Cu(110) in Acidic, Neutral and Alkaline Solutions. *ChemPhysChem* **2019**, *20* (0), 1–11. https://doi.org/10.1002/cphc.201900509.

(48) Bagger, A.; Ju, W.; Varela, A. S.; Strasser, P.; Rossmeisl, J. Electrochemical CO2 Reduction: Classifying Cu Facets. *ACS Catal.* **2019**, *9* (9), 7894–7899. https://doi.org/10.1021/acscatal.9b01899.

(49) Martínez-Hincapié, R.; Berná Galiano, A.; Rodes García, A.; Climent, V.; Feliu, J. M. Surface Acid–Base Properties of Anion-Adsorbed Species at Pt(111) Electrode Surfaces in Contact with CO2-Containing Perchloric Acid Solutions. *J. Phys. Chem. C* **2016**, *120* (29), 16191–16199. https://doi.org/https://doi.org/10.1021/acs.jpcc.6b00589.

(50) Iwasita, T.; Nart, F. C.; Rodes, A.; Pastor, E.; Weber, M. Vibrational Spectroscopy at the Electrochemical Interface. *Electrochim. Acta* **1995**, *40* (1), 53–59. https://doi.org/https://doi.org/10.1016/0013-4686(94)00239-W.

(51) Hori, Y. CO2-Reduction, Catalyzed by Metal Electrodes. In *Handbook of Fuel Cells (eds W. Vielstich, A. Lamm, H.A. Gasteiger and H. Yokokawa)*; Wiley, 2010. https://doi.org/10.1002/9780470974001.f207055.